Chinese Chemical Letters 33 (2022) 1983–1987

Contents lists available at ScienceDirect

Chinese Chemical Letters

journal homepage: www.elsevier.com/locate/cclet

Enhanced photocatalytic hydrogen production performance of pillararene-doped mesoporous TiO_2 with extended visible-light response

Haimei Wu[a], Mengyuan Wang[a], Fang Jing[a], Derui Kong[a], Yifan Chen[a,*], Chunman Jia[a,*], Jianwei Li[a,b,*]

[a] Hainan Provincial Key Laboratory of Fine Chemicals, Advanced Materials of Tropical Island Resources of Ministry of Education, College of Chemical Engineering and Technology, Hainan University, Haikou 570228, China
[b] MediCity Research Laboratory, University of Turku, Tykistökatu 6, Turku 20520, Finland

ARTICLE INFO

Article history:
Received 22 July 2021
Revised 26 September 2021
Accepted 27 September 2021
Available online 2 October 2021

Keywords:
Pillararene
Organic-inorganic hybrid materials
Visible-light photocatalysis
Water splitting
Hydrogen production

ABSTRACT

Pillararenes are a new type of supramolecular hosts, and they have been widely applied in drug delivery, catalysis, separation process, and sensors. However, they have rarely been used to produce hydrogen. Here, we report that pillararenes were used as functional molecules to explore photocatalysts and efficiently promoted hydrogen production from water. The most common and easily synthesized *p*-dimethoxy pillar[5]arene (PI-OMe) was employed to form an organic-inorganic hybrid material with titanium dioxide (TiO_2), denoted as PI-OMe-TiO_2, using a convenient sol-gel method. When the material was loaded with Pt nanoparticles, the resulting Pt/PI-OMe-TiO_2 had a good activity and stability in catalyzing water splitting to produce hydrogen under visible light. The optimized catalyst Pt/PI-OMe-TiO_2(5.2 wt%) had a photocatalytic hydrogen production rate of 1736 μmol g^{-1} h^{-1} under visible light ($\lambda > 420$ nm) irradiation. The catalyst with a Pt loading of 0.5 wt% and a PI-OMe content of 5.2 wt% also showed good long-term durability after 10 cycles of 50 h testing. The total amount of hydrogen produced was 65.01 mmol/g, and the corresponding turnover number (TON) value was 2084. Our findings suggest that pillararene derivatives are promising functional molecules to make efficient and stable hybrid photocatalysts with TiO_2 and open a new door to hydrogen production using visible light.

Sunlight-driven water splitting to produce hydrogen is considered a promising solution to the current energy crisis and environmental problems [1,2]. Since Honda and Fujishima reported that a titanium dioxide (TiO_2) electrode can photoelectrically split water into H_2 and O_2 [3], various semiconductor photocatalysts have been applied to solar-driven catalytic hydrogen production. Among these, TiO_2 has been extensively studied by scholars as a catalyst with low toxicity, low cost and good light stability. However, due to the rapid recombination of conventional TiO_2 photogenerated electron-hole (e^--h^+) pairs and the wide band gap (approximately 3.2 eV, with a corresponding excitation wavelength of shorter than 387.5 nm), its photocatalytic activity is not ideal [4]. Some strategies have sought to fully exploit solar energy and have utilized solar energy in the extended visible-light region; some strategies have used metallic or nonmetallic element (Cu [5], N [6] and P [7]) doped TiO_2, and dye-sensitized TiO_2 have exploited and applied to utilize solar energy in the extended visible-light region [8,9]. However, their low photocatalytic activity and stability greatly hinder their practical implementation. In particular, common dye-sensitized TiO_2 systems loaded with Pt nanoparticles for photocatalytic water splitting become inactivated easily and have poor stability, because the dye molecules are easily detached from the surface of the TiO_2 and degraded under light irradiation [10]. Previously, we designed and synthesized a hybrid material HO-TPA-TiO_2 based on a calix[4]arene dye HO-TPA (consisting of a 2-triphenylamine donor, an oligothiophene spacer, and a hydroxyl–substituted calix[4]arene acceptor) and TiO_2 for photocatalytic H_2 production under visible-light irradiation [11]. The HO-TPA has a cone conformation, which was beneficial for impeding intermolecular π-π aggregation, and it has four -OH groups that are able to form multiple hydrogen bonds with TiO_2. Although these properties of HO-TPA resulted in an efficient hydrogen production performance of the hybrid material, the stability of the materials was poor, as the calix[4]arene structure of the HO-TPA could flip eas-

* Corresponding authors.
E-mail addresses: chenyifan@hainanu.edu.cn (Y. Chen), jiachunman@hainanu.edu.cn (C. Jia), jianwei.li@utu.fi (J. Li).

https://doi.org/10.1016/j.cclet.2021.09.095
1001-8417/

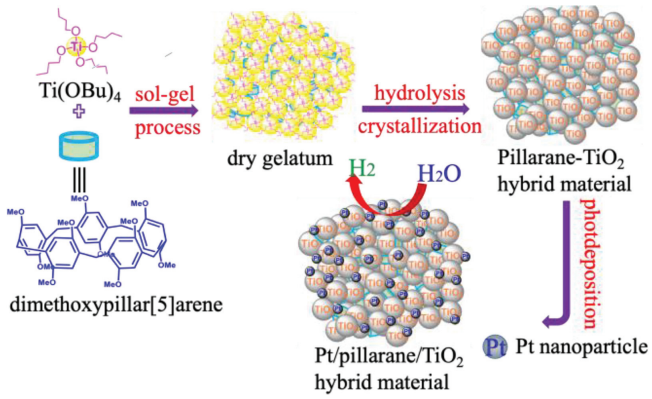

Scheme 1. Illustration of the fabrication of the PI-OMe-TiO_2.

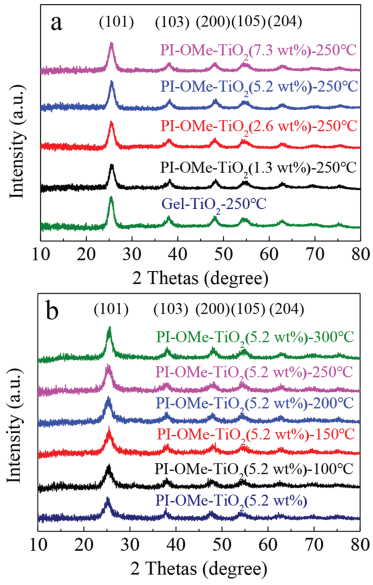

Fig. 1. The XRD patterns of PI-OMe-TiO_2 with (a) different PI-OMe content and (b) calcination at different temperature.

ily, giving rise to its various conformations, such as the cone, partial cone and 1,3-alternate [12]. Therefore, it is essential to develop functional molecules with three-dimensional structures and stable conformations that can be doped with TiO_2 to explore efficient and stable photocatalysts.

Pillararenes are a new type of macrocyclic compounds, and they have received extensive attention due to their typical columnar rigid structure and unique physical and chemical properties [13,14]. They have been employed as supramolecular hosts in a variety of applications, such as drug delivery, catalysis, separation processes and sensors [15–25]. However, it has been rarely applied in photocatalytic hydrogen production. We envisioned that the most common and easily synthesized *p*-dimethoxy pillar[5]arene (PI-OMe) [26] would be an ideal candidate to modify TiO_2 for robust photocatalytic H_2 production. First, the rigid and symmetrical pillar structure of the PI-OMe could improve the stability of the hybrid system. In addition, PI-OMe has a three-dimensional pillar cavity with rich electrons and could work as an electron transfer mediator and reservoir, facilitating the separation and transfer of photogenerated charges.

Here, we report that an organic-inorganic hybrid material was prepared from the PI-OMe and TiO_2. By loading with a co-catalyst platinum nanoparticle, the material catalyzed water splitting and produced hydrogen under visible light. The PI-OMe was used to prepare a hybrid material (PI-OMe-TiO_2) with TiO_2 *via* a convenient sol-gel method. When the material was loaded with Pt nanoparticles, the resulting Pt/PI-OMe-TiO_2 had a good activity and stability in catalyzing water splitting to produce hydrogen under visible light. The optimized catalyst Pt/PI-OMe-TiO_2(5.2 wt%) had a photocatalytic hydrogen production rate of 1736 μmol g^{-1} h^{-1} under visible light ($\lambda > 420$ nm) irradiation. The catalyst with a Pt loading of 0.5 wt% and a PI-OMe content of 5.2 wt% also showed good long-term durability after 10 cycles of 50 h testing. The total hydrogen production amount was 65.01 mmol/g, and the corresponding turnover number (TON) value was 2084. These results suggest that pillararene derivatives are promising functional molecules for forming efficient and stable hybrid photocatalysts with TiO_2 and may open a new door to hydrogen production using visible light.

The PI-OMe-TiO_2 hybrid material was prepared using the sol-gel method, as illustrated in Scheme 1. The detailed synthetic procedures have been described in the experimental section of Supporting information. Once the hybrid material PI-OMe-TiO_2 was obtained, we recorded the XRD patterns of PI-OMe-TiO_2 doped with different amounts of PI-OMe and calcined at various temperatures (Figs. 1a and b). The peaks of the PI-OMe-TiO_2 hybrid material occurred at 25.5°, 38.1°, 48.2°, 54.2° and 62.9°, respectively, corresponding to the (101), (103), (200), (105) and (204) crystal planes of anatase TiO_2. These results showed that the presence of PI-OMe in the hybrid product did not change the crystal structure of TiO_2. Calcining even at 300 °C had little effect on crystallinity, which was beneficial for removing impurities in the hybrid system, improving the cleanliness of the catalyst surface and promoting the generation and transportation of photogenerated carriers.

Figs. S1 and S2 (Supporting information) show examples of the nitrogen adsorption-desorption isotherms and the pore size distribution of the Gel-TiO_2 and PI-OMe-TiO_2(5.2 wt%) samples. The isotherms had a typical type IV pattern with a H_2-type hysteresis loop, which is an obviously characteristic of mesoporous materials. The specific surface areas of the Gel-TiO_2 and PI-OMe-TiO_2(5.2 wt%) were 174.1 m^2/g and 223.7 m^2/g, respectively. These results showed that doping PI-OMe into TiO_2 increased the BET specific surface area, and thereby improved the photocatalytic activity of the material. Moreover, the pore size was determined by the Barrett-Joyner-Halenda (BJH) method, and the pore size distributions of PI-OMe-TiO_2 (5.2 wt%) materials was predominantly centered in the mesopore region of 3.0–12 nm, which was attributed to the pore size distribution (3.3–12 nm) of the mesoporous PI-OMe and the pore size distribution (3.0–7.7 nm) of the mesoporous Gel-TiO_2. This suggests that the hybrid materials prepared through a sol-gel process featured mesoporous hierarchical structures that contributed to higher porosity. The abundant mesoporous structure shortened the transfer distance of the electrons/holes from the interior to the surface of the photocatalysts, thereby inhibiting the recombination of charges and improving the catalytic efficiency.

The thermal stability of the material was characterized by thermogravimetric (TG-DTG) tests performed on the PI-OMe-TiO_2(5.2 wt%) hybrid material and the pure PI-OMe, respectively (Fig. S3 in Supporting information). The PI-OMe was stable during the preparation process of the PI-OMe-TiO_2(5.2 wt%) hybrid material, as the calcination temperature (250 °C) was lower than the decomposition temperature of PI-OMe (284 °C). No significant quality loss of the PI-OMe-TiO_2(5.2 wt%) hybrid material was observed before 234 °C, which was presumed to be due to the removal of impurities and moisture.

The morphology and microstructure of the samples were characterized by SEM, TEM and HRTEM, as well as the element mapping. The SEM image shows that the PI-OMe-TiO_2(5.2 wt%) material was densely and disorderly packed (Fig. 2a) by nanoparti-

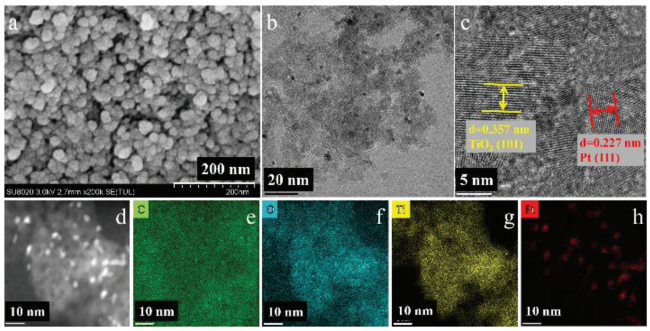

Fig. 2. (a) SEM images of PI-OMe-TiO_2(5.2 wt%); (b) TEM, (c) HRTEM, and (d-h) the elemental mappings image of Pt/PI-OMe-TiO_2(5.2 wt%).

cles with a size of approximately 10 nm (Fig. 2b). Pt nanoparticles were introduced into the hybrid material to meet the requirements of hydrogen production. The lattice spacing was approximately 0.357 nm, which was consistent with the (101) plane of anatase TiO_2, and the lattice spacing of 0.227 nm corresponded to the (111) plane of Pt (Fig. 2c). We performed the element mapping and generated EDX spectra to analyze the element composition and distribution of the PI-OMe-TiO_2(5.2 wt%) material with a platinum loading of 1.5 wt%, which allowed us to further verify the successful loading of Pt nanoparticles on the hybrid material (Fig. S4 in Supporting information). The mapping image (Figs. 2d-h) shows the uniform distribution of all elements including the precious metal Pt. The EDX analysis further confirmed the existence of Pt nanoparticles in the hybrid material.

The XPS measurements of Gel-TiO_2 and PI-OMe-TiO_2(5.2%) were performed (Fig. S5 in Supporting information). The compositions of 22% Ti, 53% O and 25% C of PI-OMe-TiO_2(5.2 wt%) with an obvious excess percentage of O, in contrast to the compositions of 24% Ti, 49% O, and 26% C of Gel-TiO_2 with the expected 1:2 ratio for Ti:O, was probably derived from the PI-OMe and air. The XPS spectrum of the platinum from the Pt/PI-OMe-TiO_2(5.2 wt%) mainly showed signals at 70.73 eV and 73.88 eV, which was attributed to Pt(0)$4f_{7/2}$ and Pt(0)$4f_{5/2}$. In addition, the peak at 72.40 eV suggested the presence of Pt^{2+} in the material. This was due to the strong interaction between the platinum and TiO_2, which induced the diffusion of Pt atoms into the TiO_2 lattice to substitute the Ti atoms and form h^+-containing defects after calcination [27,28]. These results showed that the Pt ions were successfully reduced to Pt nanoparticles and loaded on the surface of the hybrid material by attaching with TiO_2.

We recorded the solid-state UV–vis diffraction spectra of Gel-TiO_2, PI-OMe and PI-OMe-TiO_2(5.2 wt%) to evaluate the optical absorption property of the material (Fig. 3a). The Gel-TiO_2 had a strong absorption peak at approximately 316 nm, the absorption band edge was approximately 400 nm, and the corresponding band gap was 3.2 eV (Fig. 3b). In addition to the strong absorption peak at approximately 318 nm, the PI-OMe also had a weak absorption band between 350 nm and 520 nm. Interestingly, when TiO_2 and PI-OMe were combined to form a hybrid material, the optical absorption of the PI-OMe-TiO_2(5.2 wt%) extended from the ultraviolet region to 800 nm, and the absorption intensity in the visible region increased significantly. This phenomenon indicates that an obvious synergy effect exists between PI-OMe and TiO_2 in the hybrid material, which would significantly improve the visible light response ability of the hybrid. It is worth noting that the forbidden bands of PI-OMe and Gel-TiO_2 were 3.7 eV and 3.2 eV, while the PI-OMe-TiO_2(5.2 wt%) had a visible narrow forbidden band (1.7 eV) (Fig. 3b), which efficiently promoted the separation of the photogenerated charges of the hybrid from the electrons populating the position of the bottom of the conduction band (CB) and the holes

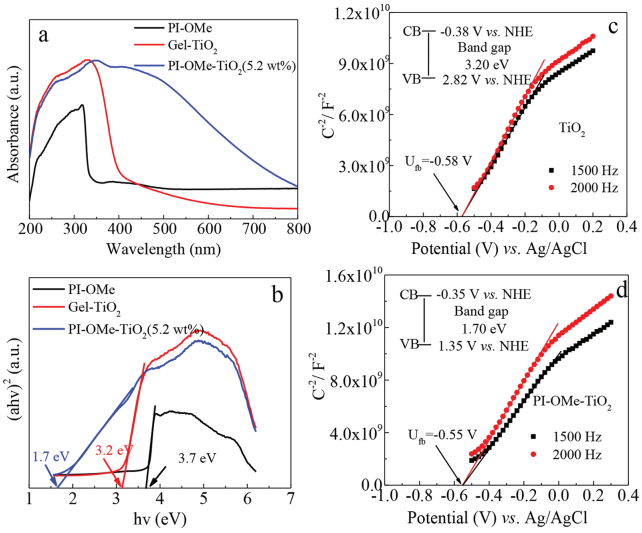

Fig. 3. The UV–vis absorption (a) and the Tauc plot (b) of PI-OMe, Gel-TiO_2 and PI-OMe-TiO_2(5.2 wt%). The Mott-Schottky plot of Gel-TiO_2 (c) and PI-OMe-TiO_2(5.2 wt%) (d).

in the valence band (VB) position upon visible-light irradiation. It is likely that a robust interaction exists between PI-OMe and TiO_2.

In order to verify the possibility of photocatalytic hydrogen production, the Mott-Schottky curves of Gel-TiO_2 and PI-OMe-TiO_2(5.2 wt%) were tested at frequencies of 1500 Hz and 2000 Hz (Figs. 3c and d). The positive slopes of the Gel-TiO_2 and PI-OMe-TiO_2(5.2 wt%) curves were consistent with those of n-type semiconductors, and their flat band potentials were −0.58 and −0.55 V *vs.* Ag/AgCl (*i.e.* −0.38 and −0.35 V *vs.* NHE). It is well-known that the flat band potential for n-type semiconductors can be regarded as approximately equal to the position of the bottom of the CB. Thus the CB potential of Gel-TiO_2 and PI-OMe-TiO_2(5.2 wt%) were estimated to be −0.38 and −0.35 V *vs.* NHE, which were more negative than the redox potential of H^+/H_2, suggesting that both of the CB positions of Gel-TiO_2 and PI-OMe-TiO_2 were enough to reduce H^+ to H_2. In fact, the hybrid exhibited excellent the photocatalytic activity compared to Gel-TiO_2 when illuminated with visible-light because of its outstanding visible-light response ability.

The photocatalytic performance of the PI-OMe-TiO_2 hybrid material loaded with 1.5 wt% Pt was studied under visible light irradiation. As shown in Fig. 4a, hydrogen production experiments were carried out on a series of Pt/PI-OMe-TiO_2 materials containing various amounts of PI-OMe ranging from 0 to 7.3 wt%. Generally, as the amounts of PI-OMe increased, the photocatalysis of the materials became more efficient. The PI-OMe-TiO_2(5.2 wt%) was the most efficient catalyst for hydrogen production and the performance reached 1.19 mmol g^{-1} h^{-1}. However, a further increase in the percentage of PI-OMe to 7.3 wt% resulted in an activity decrease to 0.97 mmol g^{-1} h^{-1}, suggesting that the photocatalytic activities of the hybrid were not simply correlated with the amount of doping with pillararene. We speculated that too many PI-OMe molecules might aggregate on the surface of TiO_2, thereby hindering effective electron transfer. In addition, the photocatalytic activity of the PI-OMe-TiO_2 hybrid material was much higher than that of the Gel-TiO_2 (0.05 mmol g^{-1} h^{-1}), which was mainly attributed to the synergy between PI-OMe and TiO_2. The photogenerated electrons in the conduction band of TiO_2 were transferred to Pt to quickly form H_2 with H^+, which promoted the positive progress of the reaction and thereby increased the hydrogen production. In addition, we also studied the effects of calcination temperature and Pt loading on hydrogen production performance of hybrid materials, as shown in Figs. S6a and S6b, respectively. The

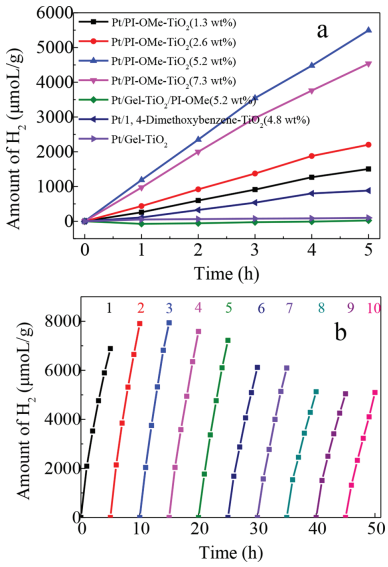

Fig. 4. (a) The photocatalytic performence of PI-OMe-TiO_2 with different PI-OMe contents for H_2 production; (b) Photocatalytic H_2 production over the recyclability of PI-OMe-TiO_2(5.2 wt%) in 20 mL H_2O/TEOA (9:1, v/v) with 0.5 wt% Pt loading under visible light irradiation ($\lambda > 420$ nm).

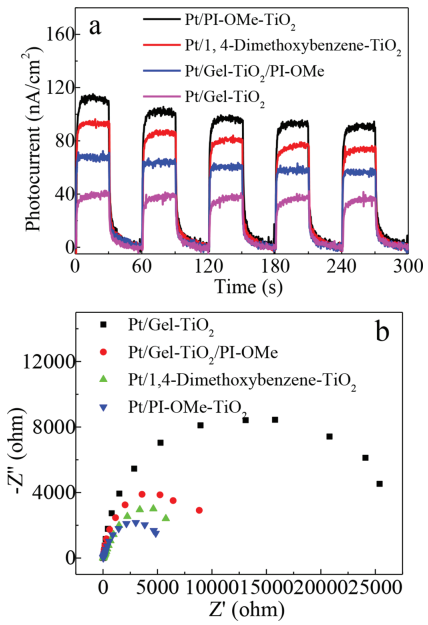

Fig. 5. (a) Photocurrent transient, and (b) EIS spectra of the photocatalysts under visible-light illumination.

results of this investigation indicate that keeping the calcination temperature (250 °C) was beneficial for promoting the preservation of photocatalytic ability with PI-OMe well preserved, and the optimal loading amount of Pt nanoparticles in the hybrid (0.5 wt%) was consistent with the most reports.

To confirm the synergistic effects of the PI-OMe and TiO_2, we first prepared a material by mechanically mixing Gel-TiO_2 and PI-OMe (5.2 wt%) (denoted as Gel-TiO_2/PI-OMe(5.2 wt%)) and then loaded 1.5 wt% Pt nanoparticles on the surface of the mixture. The hydrogen production of the materials was only 0.0046 mmol g^{-1} h^{-1}, which was approximately 260 times lower than the Pt/PI-OMe-TiO_2(5.2 wt%), even though they had the same components with the same weight percentages. In addition, the control group of 1, 4-dimethoxybenzene-TiO_2 (4.8 wt%) loaded with 1.5 wt% Pt nanoparticles was also tested for hydrogen production by photocatalytic splitting from water. Only a trace amount of H_2 was produced within 5 h. These results demonstrated that the high photocatalytic activity of the Pt/PI-OMe-TiO_2(5.2 wt%) was not only due to the components in the materials but also the unique spatial structure and the electrons storage capacity of PI-OMe. The cooperativity of the two components at the systems level resulted in the more efficient charge separation and transfer for the photocatalysis.

It is known that the reduction in H_2 production rate is a challenging problem, which could be caused by instability under light irradiation for long periods of time. The photocatalytic performance of the hybrid Pt/PI-OMe-TiO_2(5.2 wt%) photocatalysts was repeatedly evaluated to confirm their photostability in this study. The operation was the same as in the experimental section, and the photocatalyst was recycled by centrifugation, washing with deionized water and methanol and vacuum drying after every 5 h of visible light irradiation. The hybrid photocatalyst could be recycled up to 10 times. As shown in Fig. 4, generally stable H_2 production was evidently maintained until the fifth recycling reaction under visible light irradiation, and then the photocatalytic H_2 production rate of the hybrid has decreased slightly (approximately 10%) after the sixth recycle and 25% after the ninth recycle, which showed that the Pt/PI-OMe-TiO_2(5.2 wt%) material was a relatively stable photocatalyst. Based on the amounts of Pt, the turnover number (TON) of H_2 was calculated to be 2084 after 10 recycles.

We measured the photocurrent-time (*i-t*) curves to confirm the enhanced photo-response. The *i-t* curves of Pt/Gel-TiO_2, Pt/Gel-TiO_2/PI-OMe(5.2 wt%), Pt/1,4-dimethoxybenzene-TiO_2(4.8 wt%), Pt/PI-OMe-TiO_2(5.2 wt%) electrodes were detected under visible-light illumination with several on/off switches (Fig. 5a). These curves show that the photocurrent response of the Pt/PI-OMe-TiO_2(5.2 wt%) samples were higher than those of the other materials. The density of the samples followed the sequence: Pt/Gel-TiO_2 < Pt/Gel-TiO_2/PI-OMe < Pt/1,4-dimethoxybenzene-TiO_2 < Pt/PI-OMe-TiO_2, which indicates that the photogenerated charges separation efficiency of the hybrid material was significantly improved under visible light irradiation, and more effective interfacial electrons transfer occurred between the pillararene and TiO_2 in the hybrid system to further improve the photocatalytic activity. In Fig. S7 (Supporting information), the comparison of the photocurrent transient spectra of PI-OMe-TiO_2(5.2 wt%) and Pt/PI-OMe-TiO_2(5.2 wt%) illustrates that Pt nanoparticles on the surface of the hybrid PI-OMe-TiO_2(5.2 wt%) would effectively facilitate the photogenerated charges separation. Moreover, the electrochemical impedance spectra (EIS) of Pt/Gel-TiO_2, Pt/Gel-TiO_2/PI-OMe(5.2 wt%), Pt/1,4-dimethoxybenzene-TiO_2(4.8 wt%), and Pt/PI-OMe-TiO_2(5.2 wt%) were obtained using a three electrode cell system under visible-light illumination to investigate the relationship between the transfer resistance of the charge carriers and the photocatalytic activity of the hybrid (Fig. 5b). In the EIS plots, Pt/PI-OMe-TiO_2(5.2 wt%) had the smallest arc radius of all the samples. The arc radii of the samples followed the following sequence and were in accordance with the results of their photocatalytic performance: Pt/Gel-TiO_2 > Pt/Gel-TiO_2/PI-OMe > Pt/1,4-dimethoxybenzene-TiO_2 > Pt/PI-OMe-TiO_2. It indicates that the lower charge-carriers transfer resistance and faster interface charge-carriers migration exist at PI-OMe/TiO_2/electrolyte interface.

Steady-state solid photoluminescence (PL) spectra were generated to monitor the electron transfer from excited PI-OMe* to TiO_2 and to enable the investigation of the photocatalytic mechanism of the hybrid material PI-OMe-TiO_2 catalysts (Fig. S8 in Support-

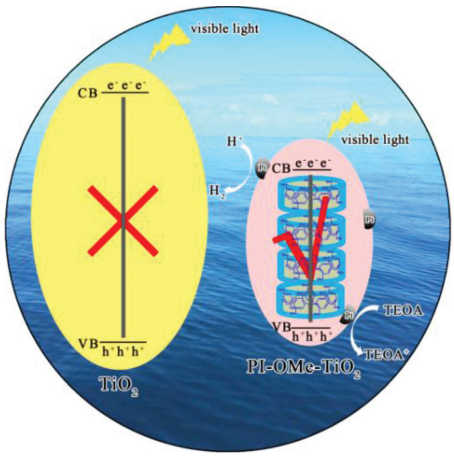

Fig 6. The proposed mechanism for the photocatalytic hydrogen production of the PI-OMe-TiO_2.

ing information). The PI-OMe showed an intensive emission peak at 423 nm, which was ascribed to its strong recombination of excited charge pairs. For comparison, the PL spectra of the other samples under the same conditions showed a decrease in intensity, in the following order: PI-OMe > physical-mixing gel-TiO_2/PI-OMe > PI-OMe-TiO_2. This indicated that more efficient charges transport occurred at the interface between the PI-OMe and TiO_2 in the PI-OMe-TiO_2 hybrid than that in the physical-mixing system and the pure PI-OMe. In addition, the averaged decay time of the catalysts verified the above PL quenching results (Fig. S9 in Supporting information). The PI-OMe exhibited the longest averaged decay time of 1000 ps. With the incorporation of TiO_2, the averaged decay time was shortened to 37.7 ps for the physical mixture and 26.6 ps for PI-OMe-TiO_2, respectively. Pt NPs are commonly used as co-catalysts and are loaded on the surface of the hybrid materials PI-OMe-TiO_2 by photodeposition. A Schottky barrier can be formed at the interface between the Pt NPs and the hybrid PI-OMe-TiO_2. The photogenerated electrons therefore passed through the Schottky barrier to the surface of the PI-OMe-TiO_2 photocatalyst and were captured by the cocatalyst, which functioned as a hydrogen generation site to photoreduce H^+ to form H_2. Herein, series of characterizations displayed that the effective synergy effect between on PI-OMe and TiO_2, which endowed the hybrid with the largely expand visible-light response range and the obviously enhanced visible-light absorption intensity. We can conclude that the PI-OMe effectively and essentially regulated the band gaps of the TiO_2 in the hybrid. The PI-OMe inherently functioned as the photogenerated electron transporting channels and reservoir, due to its three-dimensional pillar cavity with rich electrons. In contrast, pure TiO_2 could not exhibit effective photocatalytic functioning under illumination with visible light, which further illustrates that the synergy effect between PI-OMe and TiO_2 in the hybrid PI-OMe-TiO_2 effectively promotes the photocatalytic activity under visible-light illumination (Fig. 6).

In summary, we have successfully prepared a stable hybrid material composed of TiO_2 and a pillararene derivative using the convenient sol-gel method. A tight interface was formed between the two components, and when platinum nanoparticles were loaded as a co-catalyst, this resulted in high-efficiency and long-lasting photocatalytic activity. The PI-OMe-TiO_2 doped with different amounts of PI-OMe all showed better photocatalytic performance than the pure TiO_2 material. Among these, the Pt/PI-OMe-TiO_2(5.2 wt%) had the highest efficiency of H_2 production, 1736 μmol g^{-1} h^{-1}. We attribute the excellent photocatalytic performance of the PI-OMe-TiO_2 hybrid material to its interfacial synergistic effect, effective charge separation and transfer between TiO_2 and PI-OMe, as well as its robust light absorption ability. In contrast, under similar photocatalytic conditions, the PI-OMe-TiO_2 hybrid material had a much higher hydrogen production activity and better stability than the similar surface sensitizing TiO_2 system. The hybrid material also exhibited remarkable stability after a reaction time of 50 h. Our findings suggested that a pillararene derivative could be an ideal modifier for effectively promoting the photocatalytic performance of TiO_2. Since pillararene is a supramolecular host, our lab plans to introduce proper supramolecular guest molecules into the photocatalytic systems to explore more efficient photocatalysts for water splitting in particular and chemical reactions in general.

Declaration of competing interest

The authors declare that they have no known competing financial interests or personal relationships that could have appeared to influence the work reported in this paper.

Acknowledgments

We are grateful for the financial support from the Natural Science Foundation of Hainan Province, China (No. 219QN151), the National Natural Science Foundation of China (No. 21801052), the Hainan University Start-up fund (No. KYQD(ZR)1852) and the construction program of research platform in Hainan University (No. ZY2019HN09).

Supplementary materials

Supplementary material associated with this article can be found, in the online version, at doi:10.1016/j.cclet.2021.09.095.

References

[1] S. Sato, T. Morikawa, S. Saeki, T. Kajino, T. Motohiro, Angew. Chem. 122 (2010) 5227–5231.
[2] H. Park, H. Kim, G. Moon, W. Choi, Energy Environ. Sci. 9 (2016) 411–433.
[3] A. Fujishima, K. Honda, Nature 238 (1972) 37–38.
[4] K. Nakata, A. Fujishima, J. Photoch. Photobio. C 13 (2012) 169–189.
[5] L. Samet, K. March, N. Brun, et al., Mater. Res. Bull. 107 (2018) 1–7.
[6] S. Ida, P. Wilson, B. Neppolian, et al., Ultrason. Sonochem. 57 (2019) 62–72.
[7] Q. Liu, J. Shen, X. Yu, et al., Appl. Catal. B: Environ. 248 (2019) 84–94.
[8] X. Zhang, T. Peng, S. Song, J. Mater. Chem. A 4 (2016) 2365–2402.
[9] M.D. Brady, R.N. Sampaio, D. Wang, T.J. Meyer, G.J. Meyer, J. Am. Chem. Soc. 139 (2017) 15612–15615.
[10] A. Kruth, A. Quade, V. Bruser, K.D. Weltmann, J. Phys. Chem. C. 117 (2013) 3804–3811.
[11] Y.F. Chen, J.F. Huang, M.H. Shen, et al., J. Mater. Chem. A 7 (2019) 19852–19861.
[12] P. Lhoták, A. Bílá, J. Budka, M. Pojarová, I. Stibor, Chem. Commun. (2008) 1662–1664.
[13] Y. Yao, Y. Wang, F. Huang, Chem. Sci. 5 (2014) 4312–4316.
[14] T. Ogoshi, T. Yamagishi, Chem. Commun. 50 (2014) 4776–4787.
[15] G. Yu, M. Xue, Z. Zhang, et al., J. Am. Chem. Soc. 134 (2012) 13248–13251.
[16] G. Yu, X. Zhou, Z. Zhang, et al., J. Am. Chem. Soc. 134 (2012) 19489–19497.
[17] Y. Yao, M. Xue, J. Chen, M. Zhang, F. Huang, J. Am. Chem. Soc. 134 (2012) 15712–15715.
[18] L. Chen, W. Si, L. Zhang, et al., J. Am. Chem. Soc. 135 (2013) 2152–2155.
[19] Q. Duan, Y. Cao, Y. Li, et al., J. Am. Chem. Soc. 135 (2013) 10542–10549.
[20] H. Guo, X. Yan, B. Lu, et al., J. Mater. Chem. C 8 (2020) 15622–15625.
[21] Y. Cao, Y. Chen, Z. Zhang, et al., Chin. Chem. Lett. 32 (2021) 349–352.
[22] R. Zhang, X. Yan, H. Guo, et al., Chem. Commun. 56 (2020) 948–951.
[23] M. Cen, Y. Ding, J. Wang, et al., ACS Macro. Lett. 9 (2020) 1558–1562.
[24] Y. Cai, Z. Zhang, Y. Ding, et al., Chin. Chem. Lett. 32 (2021) 1267–1279.
[25] Z. Zhang, Y. Luo, J. Chen, et al., Angew. Chem. Int. Ed. 50 (2011) 1397–1401.
[26] T. Ogoshi, T. Aoki, K. Kitajima, et al., J. Org. Chem. 76 (2011) 328–331.
[27] J.A. Horsley, J. Am. Chem. Soc. 101 (1979) 2870–2874.
[28] C. Xu, X. Lai, G.W. Zajac, et al., Phys. Rev. B 56 (1997) 13464–13482.